Journal of Hazardous Materials 485 (2025) 136499

Contents lists available at ScienceDirect

Journal of Hazardous Materials

journal homepage: www.elsevier.com/locate/jhazmat

Mercury speciation and stable isotopes in emperor penguins: First evidence for biochemical demethylation of methylmercury to mercury-dithiolate and mercury-tetraselenolate complexes

Alain Manceau [a,b,*], Paco Bustamante [c], Etienne Richy [c], Yves Cherel [d], Sarah E. Janssen [e], Pieter Glatzel [a], Brett A. Poulin [f]

[a] European Synchrotron Radiation Facility (ESRF), 38000 Grenoble, France
[b] ENS de Lyon, CNRS, Laboratoire de Chimie, 69342 Lyon, France
[c] Littoral Environnement et Sociétés (LIENSs), CNRS-La Rochelle Université, 17000 La Rochelle, France
[d] Centre d'Etudes Biologiques de Chizé (CEBC), CNRS-La Rochelle Université, 79360 Villiers-en-Bois, France
[e] US. Geological Survey, Upper Midwest Water Science Center, Madison, WI 53562, USA
[f] Department of Environmental Toxicology, University of California Davis, Davis, CA 95616, USA

HIGHLIGHTS

- HERFD-XANES spectra, and Hg and N stable isotopes were measured in emperor penguins.
- This is the first evidence for two demethylation pathways: MeHg → $Hg(Sec)_4$ and MeHg → $Hg(SR)_2$.
- $Hg(Sec)_4$ and $Hg(SR)_2$ have distinct species-specific $\delta^{202}Hg(Sec)_4$ and $\delta^{202}Hg(SR)_2$ values.
- Calculation of the *effective* Se:Hg molar ratio shows absence of Se deficiency.
- Egg albumen contains 100 % MeHg and the yolk contains 32 % MeHg and 68 % $Hg(Sec)_4$.

GRAPHICAL ABSTRACT

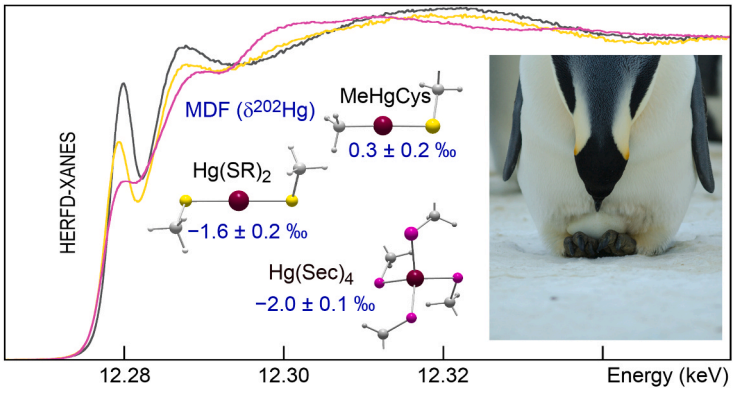

ARTICLE INFO

Keywords:
Mercury
HERFD-XANES
Isotope fractionation
Toxicology
Bird

ABSTRACT

Apex marine predators, such as toothed whales and large petrels and albatrosses, ingest mercury (Hg) primarily in the form of methylmercury (MeHg) via prey consumption, which they detoxify as tiemannite (HgSe). However, it remains unclear how lower trophic level marine predators, termed mesopredators, with elevated Hg concentrations detoxify MeHg and what chemical species are formed. To address this need, we used high energy-resolution X-ray absorption near edge structure spectroscopy paired with nitrogen (N) and Hg stable isotopes to identify the chemical forms of Hg, Hg sources, and species-specific $\delta^{202}Hg$ isotopic values in emperor penguin, a mesopredator feeding primarily on Antarctic silverfish. The penguin liver contains variable proportions of MeHg and two main inorganic Hg complexes (IHg), Hg-dithiolate ($Hg(SR)_2$) and Hg-tetraselenolate ($Hg(Sec)_4$), each characterized by specific isotopic values ($\delta^{202}MeHg = 0.3 \pm 0.2$ ‰, $\delta^{202}Hg(SR)_2 = -1.6 \pm 0.2$ ‰, $\delta^{202}Hg(Sec)_4$

* Corresponding author at: European Synchrotron Radiation Facility (ESRF), 38000 Grenoble, France.
E-mail address: alain.manceau@ens-lyon.fr (A. Manceau).

https://doi.org/10.1016/j.jhazmat.2024.136499
Received 11 September 2024; Received in revised form 26 October 2024; Accepted 11 November 2024
Available online 13 November 2024

= −2.0 ± 0.1 ‰). Using $\delta^{15}N$ as a tracer of food source, we show that $Hg(SR)_2$ is likely not obtained through dietary intake, but rather is present as a biochemical demethylation product. Furthermore, on average, female penguins transferred Hg to the egg strictly as MeHg in the egg albumen but as mixtures of MeHg and IHg in the membrane (89 % and 11 %, respectively) and yolk (32 % MeHg and 68 % $Hg(Sec)_4$). Despite IHg species in eggs, MeHg is still the main species quantitatively transferred by the mother to the chick because of the disproportionate mass of the MeHg-rich albumen compared to the yolk. This work highlights the transformation of MeHg to $Hg(SR)_2$ during demethylation for the first time in multicellular organisms, but further work is needed to understand the formation of $Hg(SR)_2$ in the presence of relatively abundant Se biomolecules in lower trophic level predator species.

1. Introduction

Mercury (Hg) released to the atmosphere by human activity can impact fauna in remote regions of Antarctica and has been persistent interest for the research community since the late 1980s [1–7]. Early studies focused on Hg concentration in seabirds and marine mammals [8–10]. Norheim (1987) [1] observed a positive correlation between Hg and selenium (Se) in birds, including penguins, which was suggested to decrease Hg toxicity, a hypothesis that has since been widely confirmed [11–25]. Starting in 2015, the field of research on Hg contamination in Antarctica and the Southern Ocean has been broadened with the use of mass independent fractionation (MIF, $\Delta^{199}Hg$, $\Delta^{200}Hg$, $\Delta^{201}Hg$) and mass dependent fractionation (MDF, $\delta^{202}Hg$) of Hg stable isotopes [26–33].

Hg undergoes MIF through photochemical reduction of Hg(II) to Hg (0) and photodemethylation of organic methylmercury (MeHg) to inorganic mercury (IHg) [34–37]. In the context of marine research, MIF has been used to trace the vertical and lateral movement of animals in the oceans [26,38–40]. $\Delta^{199}Hg$ values decrease when light diminishes in the water column due to less photochemical demethylation, which provides insight into the foraging depth, foraging latitude (due to sea ice extent), and trophic source of marine biota [39,41–45]. Using $\Delta^{199}Hg$ as an ecological tracer, Jung et al. [33] observed in 2024 that emperor penguins (*Aptenodytes forsteri*, EP) from Coulman Island and Cape Washington in the Ross Sea forage at deeper depth (> 200 m) than Adélie penguins (*Pygoscelis adeliae*, AP) from Cape Hallett. EP feed primarily on Antarctic silverfish (*Pleuragramma antarcticum*) and secondarily on squid (*Psychroteuthis glacialis)*, which dominate the prey biomass at depths exceeding 200 m (mesopelagic zone), whereas AP feed primarily on euphausiids (Antarctic krill *Euphausia superba* and crystal krill *E. crystallorophias*) in subsurface waters (photic epipelagic zone) [46–48]. Analysis of stomach contents showed that 89–95 % of the EP prey are silverfish at Cape Washington [46]. Thus, EP feed at a higher trophic level than AP, which is reflected in the elevated total Hg concentrations in liver, kidney, heart and skeletal muscle that are, on average, four times higher than those measured in AP (1.3 versus 0.3 μg/g dry weight, respectively) [33]. This variation in trophic level was also independently confirmed using nitrogen isotopic composition ($^{15}N/^{14}N$, $\delta^{15}N$), an indicator of trophic position in the food web structure and for foraging ecology [49–52]. The blood of EP at Adélie Land were found to be enriched in $\delta^{15}N$ (12.0 ± 0.4 ‰) compared to AP (7.9 ± 0.1 ‰) [47]. The difference was explained by the distinct dietary pathways of the two penguins, as difference in $\delta^{15}N$ value of 4.1 ‰ was similar to the difference in ^{15}N value between Antarctic silverfish ($\delta^{15}N$ = 10.6 ± 0.3 ‰) and Antarctic and ice krill ($\delta^{15}N$ = 5.5 ± 0.4 and 6.8 ± 0.7 ‰, respectively). While the combination of $\Delta^{199}Hg$ and $\delta^{15}N$ can provide key information regarding dietary habits [28], it is more difficult to decipher internal Hg processes.

In contrast to MIF, MDF of Hg can be used to trace metabolic processes, such as methylation and demethylation reactions within and between tissues of seabirds and marine mammals [31,53–56]. Due to kinetic isotope effects, the product of the reaction is enriched in the lighter ^{198}Hg isotope relative to heavier ^{202}Hg, and therefore has a lower ^{202}Hg to ^{198}Hg ratio ($\delta^{202}Hg$). Jung et al. [33] observed a significant linear relationship between the percentage of MeHg (%MeHg) and $\delta^{202}Hg$ across the tissues of EP and AP. Furthermore, there was a hierarchy in the extent of demethylation among the liver, kidney and skeletal muscle based on Hg concentrations: liver ([Hg] = 2.1 ± 0.6 μg/g, $\delta^{202}Hg$ = 0.07 ‰, %MeHg = 69 ± 8) > kidneys ([Hg] = 1.1 ± 0.2 μg/g, $\delta^{202}Hg$ = 0.27 ‰, %MeHg = 75 ± 11) > skeletal muscle ([Hg] = 0.8 ± 0.2 μg/g, $\delta^{202}Hg$ = 0.78 ‰, %MeHg = 87 ± 12). While these measurements provide insight to the Hg demethylation process, Hg stable isotope measurements alone do not resolve the inorganic Hg species byproducts.

The research on Hg contamination in the Southern Ocean has been extended further in 2021 with the application of high energy-resolution fluorescence detected (HERFD) X-ray absorption near-edge structure (XANES) spectroscopy to examine the coordination structure of Hg in giant petrels (both *Macronectes giganteus* and *M. halli*) from the Kerguelen Islands and Adélie Land and in south polar skua (*Stercorarius maccormicki*) from Cape Hallett [55,57]. In giant petrels, it was shown that MeHg is detoxified to chemically inert Hg selenide (HgSe) following the stepwise demethylation reaction methylmercury cysteine (MeHg-Cys) → tetraselenolate ($Hg(Sec)_4$) → HgSe [57]. The tetraselenolate complex $Hg(Sec)_4$ is thought to be bound predominantly to selenoprotein P (SelP) [58], a protein produced mainly in the liver and secreted into the systemic circulation to transport Se to extra-hepatic tissues [20,59,60].

Formation of the intermediate $Hg(Sec)_4$ complex in the detoxification of MeHg has unwelcome implications. It depletes the pool of bioavailable Se needed for selenoenzyme synthesis and activity, because four Se atoms are required to demethylate just one MeHg. The $Hg(Sec)_4$ complex also needs to be considered in the calculation of the Se:Hg molar ratio commonly used as a metric estimate of the toxicological risk associated with Hg exposure. It is largely accepted that a Se:Hg ratio below 1:1 is hazardous and that organisms are more protected against Hg toxicity when the ratio rises above 1 [19]. The paradigm behind this threshold is the higher bonding affinity of Hg to Se than sulfur (S), commonly observed during the detoxification of MeHg to the chemically inert HgSe in high trophic level cetaceans and seabirds [11,12,57,61–69]. Another piece of supporting evidence for the high selenophilicity of Hg is the rapid exchange of thiolate ligands for selenolate ligands in aqueous medium [70–73]. However, if $Hg(Sec)_4$ is the only Hg-Se coordination structure, then the threshold value of 1 is reached when Se:Hg = 4. Omitting $Hg(Sec)_4$, which cannot effectively be assessed using chemical analyses, in the Se:Hg calculation leads to an underestimate of the toxicity of Hg and an overestimation of the amount of Se that is bioavailable. Keeping the practicable threshold of 1, while accounting for $Hg(Sec)_4$, is possible by replacing the chemical molar concentration of Se ($[Se]_{chem}$) in the calculation of the Se:Hg ratio by its *effective* molar concentration ($[Se]_{eff}$) defined as follows [57].

$$[Se]_{chem}:[Hg] = [Se]_{eff}:[Hg] \times (f(HgSe) + 4 \times f(Hg(Sec)_4)) \quad (1)$$

where concentrations are expressed in molarity and f(HgSe) and f(Hg $(Sec)_4$ are the fractions of each Hg complex. Se is in excess when $[Se]_{eff}$:[Hg] > 1 and deficient when $[Se]_{eff}$:[Hg] < 1. The concentration of bioavailable Se is.

$$[Se]_{bio} = (1 - [Hg]:[Se]_{eff}) \times [Se]_{chem} \quad (2)$$

where [Hg]:[Se]$_{eff}$ is the fraction of Se bound to Hg. Thus, besides allowing quantitative determination of the Hg chemical forms, HERFD-XANES also allows for the evaluation of Hg-induced Se deficiency.

Combining HERFD-XANES and isotope analyses has demonstrated that species-specific values can be assessed for δ^{202}MeHg, δ^{202}Hg(Sec)$_4$ and δ^{202}HgSe in giant petrels and revealed that Hg(Sec)$_4$ was depleted in ^{202}Hg (δ^{202}Hg(Sec)$_4$ = −1.37 ± 0.06 ‰) relative to MeHg (δ^{202}MeHg = 2.69 ± 0.04 ‰), and HgSe was enriched in ^{202}Hg (δ^{202}HgSe = 0.18 ± 0.02 ‰) relative to Hg(Sec)$_4$ [31]. Furthermore, Jung et al. [33] used the giant petrel results to infer that MeHg was demethylated as Hg(Sec)$_4$ in penguins. However, this relevant interpretation is not unequivocal. Although MeHg, Hg(Sec)$_4$, and HgSe were the only Hg forms identified in the liver, kidney, brain and muscle tissues of giant petrels (the blood had some Hg(SR)$_2$), Hg-dithiolate (Hg(SR)$_2$) was co-present with Hg (Sec)$_4$ in the kidney and muscle tissues of Clark's grebe (*Aechmophorus clarkii*), a waterbird from California [55]. Furthermore, the measured δ^{202}Hg values correlated linearly with the sum of the two IHg forms. There was no indication that δ^{202}Hg(Sec)$_4$ differed from δ^{202}Hg(SR)$_2$, making the two structural forms impossible to distinguish using stable Hg isotopes. Because EP is a mesopredator, akin to the Clark's grebe, we propose Hg(SR)$_2$ coexists with Hg(Sec)$_4$ within the organism. If Hg(SR)$_2$ is present, then one should be able to infer if it is a demethylation product, since EP feed primarily on fish and secondarily on squid, which both are known to contain almost exclusively MeHg [74–77]. AP is not an ideal choice to address this question since Antarctic krill, their main prey, has a large proportion of IHg (> ~75 %) [78–80]. This dietary form, likely Hg(SR)$_2$, would not be distinguished from the demethylation form(s) of Hg in AP.

The present study was undertaken to (1) extend our understanding of MeHg detoxification from previously studied high trophic level predators to relatively understudied mesopredators using EP as a study organism, (2) evaluate to what extent tissue Hg burdens and chemical forms deplete bioavailable Se, and (3) use complementary isotope and Hg coordination structure data to assess how detoxification reactions influence maternal transfer of Hg. The presentation of the results is organized as follows. First, Hg and Se concentrations in body tissues (liver and muscle) of EP males and females and in EP eggs (membrane, albumen and yolk) are presented, providing baseline information for further Hg speciation and isotopic analysis. Second, HERFD-XANES is used to identify the demethylated forms of Hg and to calculate the concentration of bioavailable Se from the *effective* Se:Hg molar ratio. Third, the species-specific δ^{202}Hg(Sec)$_4$ and δ^{202}Hg(SR)$_2$ values are determined from coupled HERFD-XANES and Hg isotope measurement. Lastly, the Hg complexes transferred to chick embryos in egg membrane, albumen, and yolk are determined indirectly from the Hg isotope values (δ^{202}Hg, δ^{202}Hg(Sec)$_4$, δ^{202}Hg(SR)$_2$), as the Hg concentration in eggs is too low to permit direct HERFD-XANES identification.

2. Materials and methods

2.1. Sample collection

Soft tissues (liver and muscle) and eggs (membrane, albumen, yolk) of EP were collected at Adélie Land (66°40'S, 140°00'E) from 18 EP and 18 eggs. Thirteen specimens were healthy adult females that died naturally in the colony following an evagination of the genital tract during egg-laying in May (EP are winter breeders, unlike AP). The five other individuals (two females and three males) were also found dead in the colony, but later in the breeding cycle, between June and September. Given the small number of individuals found dead each year, sampling took place between 2008 and 2014. The individuals were dissected on site and pectoral muscle and liver were frozen and stored at −20 °C until analysis. The sampled eggs were freshly abandoned eggs that were collected in May 2010, 2011, and 2014. The eggs were transported to France whole, and the membrane, albumen and yolk were separated in the laboratory and freeze-dried.

2.2. Hg and Se analyses

Total Hg (THg) of the soft tissues and egg components was analyzed by atomic absorption spectrophotometry with an Advanced Mercury Analyzer (AMA-254 Altec®) on dry powder [81]. A split of the samples was microwave digested with 4 mL of Suprapur® nitric and chloric acid (Merck) in 3:1 ratio, and Se analyzed by Inductively Coupled Plasma Mass Spectrometry (ICP-MS II Series Thermo Fisher Scientific®). Quality assurance and quality control (QA/QC) were assessed by procedural blanks and analysis of certified reference materials. Recoveries were 99.6 ± 0.9 % (n = 15) for Hg (TORT-2, National Research Council Canada [NRCC] and 108 ± 3 % (n = 4) for Se (DOLT-4, NRCC). Chemical analysis of MeHg was performed on soft tissues and egg components using a nitric acid (4.5 M) extraction followed by analysis using chemical ethylation, gas chromatography separation, and cold vapor atomic fluorescence detection [82]. Analyses had acceptable certified reference material recoveries (91.3 ± 5.7 %, n = 7, International Atomic Energy Agency [IAEA] 407) and replicate measurements (< 3 % variability between triplicates, n = 5).

2.3. N isotopic measurement

Liver and muscle samples were freeze-dried and powdered. Subsamples were weighed with a microbalance, packed in tin containers, and N isotope ratios were subsequently determined by a continuous flow mass spectrometer (Delta V Advantage with a Conflo IV interface, Thermo Scientific) coupled to an elemental analyzer (Flash 2000, Thermo Scientific). Stable isotope concentrations were expressed in conventional notation ($\delta X = [R_{sample} / R_{standard}) - 1]$ x 1000) where X is ^{15}N and R is the corresponding ^{15}N/^{14}N ratio. $R_{standard}$ is atmospheric N_2 (air). Replicate measurements of internal laboratory standards (acetanilide and peptone) indicate a measurement error < 0.15 ‰.

2.4. Hg isotopic measurement

Tissues were analyzed for Hg stable isotopes at the U.S. Geological Survey Mercury Research Laboratory. Briefly, dried tissues were digested in concentrated nitric acid for eight hours at 90 ℃. After the initial digestion, a 10 % (v/v) addition of bromine monochloride was added and the digest solution was heated for an additional two hours to ensure degradation of organic matter. Sample digestions were diluted to an acid content of < 10 % and a concentration of 0.50–0.75 ng mL^{-1} prior to analysis of Hg stable isotopes using a multicollector inductively coupled plasma mass spectrometer (MC-ICP-MS, Thermo Scientific, Neptune Plus). Analysis and introduction parameters for the MC-ICP-MS are outlined elsewhere [83]. Samples were analyzed using standard-sample bracketing with National Institute of Standards and Technology (NIST) 3133 and reported in standard delta notation [84]. Secondary standard (NIST RM 8610, "UM-Almadén") and certified reference materials (IAEA 407 and DOLT-3, NRCC) were run alongside samples and produced comparable Hg isotope results to literature values (Table S1) [31,55,85,86].

2.5. HERFD-XANES measurement and analysis

Hg L_3-edge XANES spectra were measured at the European Synchrotron Radiation Facility (ESRF) on the ID26 beamline [87] in high energy resolution fluorescence detection mode (HERFD) [88–90]. The intensity of the Hg Lα1 line was measured by means of the Si(555) reflection of five crystals of 10 cm diameter spherically bent to a radius of 0.5 m [91]. The photon energy was calibrated by assigning the maximum of the near-edge structure of the MeHg-cysteine complex to 12279.8 eV for consistency with our previous studies. Spectra were collected at a temperature of 10–15 K and a scan time of 5 s to reduce exposure, and repeated at different pristine positions on the sample to increase the signal-to-noise ratio. Multiple X-ray absorption scans were

averaged with PyMCA [92].

Data reduction and analysis were carried out as previously described [57,58], using the suite of Labview computer programs from 10.3.2 at the Advanced Light Source (Berkeley, USA). The nature and molar proportions of the Hg complexes were obtained using principal component analysis (PCA), target transformation (TT) of our previously published library of reference spectra, and linear combination fitting (LCF) of the multi-component HERFD-XANES spectra to reference spectra positively identified by TT [85,93,94]. The database includes the main coordination structures of Hg discussed in the literature (MeHg-Cys, $Hg(Cys)_2$, MeHgSec, $Hg(Sec)_2$, $Hg(Sec)_4$) [95–98]. The quality of a Hg reference tested by TT was evaluated by computing its SPOIL value [99]. Values ≤ 1.5 were considered excellent, 1.6–3.0 good, 3.1–4.5 fair, and > 4.5 poor. The quality of the LCF was estimated using the normalized sum-squared difference between the experimental and fit spectra expressed as $NSS = \Sigma[(y_{exp}\text{-}y_{fit})^2]/\Sigma(y_{exp}^2)$. The precision of estimation of a fit component was estimated to be equal to the variation of its value when the fit residual (*NSS*) was increased by 20 %. The difference between %MeHg determined by chemical analysis (see methods above) and spectroscopy is within precision of the two independent methods (Fig. S1). Consistency between %MeHg determined by the two independent methods served as internal consistency check for the reliability of the complexation analysis by HERFD-XANES. All liver data and MeHg, $Hg(SR)_2$, and $Hg(Sec)_4$ spectra are provided in the Supporting Information (Table S2).

3. Results and discussion

3.1. Bioaccumulation of Hg, MeHg, and Se in liver, muscle and eggs

THg concentrations in tissues ($n = 18$) and eggs ($n = 18$) range from 1.1 to 5.1 μg/g in liver (<[Hg]> = 2.3 ± 1.1 μg/g; avg ± stdev), 0.4 to 0.8 μg/g in muscle (<[Hg]> = 0.6 ± 0.1 μg/g), 0.2 to 0.7 μg/g in the egg albumen (<[Hg]> = 0.4 ± 0.1 μg/g), 0.06 to 0.14 μg/g in the yolk (<[Hg]> = 0.09 ± 0.02 μg/g), and 0.03 to 0.11 μg/g in the membrane (<[Hg]> =0.08 ± 0.02 μg/g) (Fig. 1, Table S3). Selenium concentrations in the tissues and eggs range from 6.0 to 33.6 μg/g in liver (<[Se]> = 13.8 ± 8.1 μg/g), from 3.5 to 9.9 μg/g in muscle (<[Se]> = 4.8 ± 1.7 μg/g), from 5.5 to 8.8 μg/g in egg membrane (<[Se]> = 7.3 ± 1.0 μg/g), from 5.7 to 8.4 μg/g in egg albumen (<[Se]> = 7.0 ± 0.8 μg/g), and from 1.8 to 3.3 μg/g in egg yolk (<[Se]> = 2.4 ± 0.4 μg/g). Molar ratios between Se and Hg decrease in the following order: membrane (<Se:Hg> = 258 ± 66) > yolk (<Se:Hg> = 72 ± 18) > albumen (<Se:Hg> = 43 ± 10) > muscle (<Se:Hg> = 21 ± 6) > liver (<Se:Hg> = 17 ± 11) (Fig. 1a). The molar ratio of Se:Hg is always above 1 in the liver with a minimum value of 6.1 in the liver of EP06, which has the highest THg concentration (5.1 μg/g). This individual also has the second lowest MeHg level (16 % MeHg by chemical analysis), suggesting some proportion of the IHg is a demethylation product. This hypothesis is further supported by the overall decrease in %MeHg with greater THg concentration in the albumen (100 ± 0 %), muscle (89 ± 4 %), and liver (30 ± 10 %, Fig. 1b).

The THg concentrations of adult EP from Adélie Land are within the range of literature values most commonly reported for chicks [2–4,27,28,33,100–107], and reviewed recently by Gimeno et al.[7] For example, EP chicks from the Ross Sea studied by Jung et al.[33] have [Hg] = 2.1 ± 0.6 μg/g in liver and [Hg] = 0.8 ± 0.2 μg/g in the muscle tissue, which is comparable to the values measured in the adult EP from this study ([Hg] = 2.3 ± 1.1 μg/g and [Hg] = 0.6 ± 0.1 μg/g, respectively). Our results appear contradictory with the bioaccumulation of Hg, which often increases as a function of age and higher trophic position [108–111]. The similarities in Hg concentrations between chicks and adults potentially relates to the high variability of the environmental Hg concentrations in the Southern Ocean with notably elevated concentrations in the Ross Sea due to volcanic activity and the likely release of Hg sulfide in this area [80,112,113]. A recent study using AP

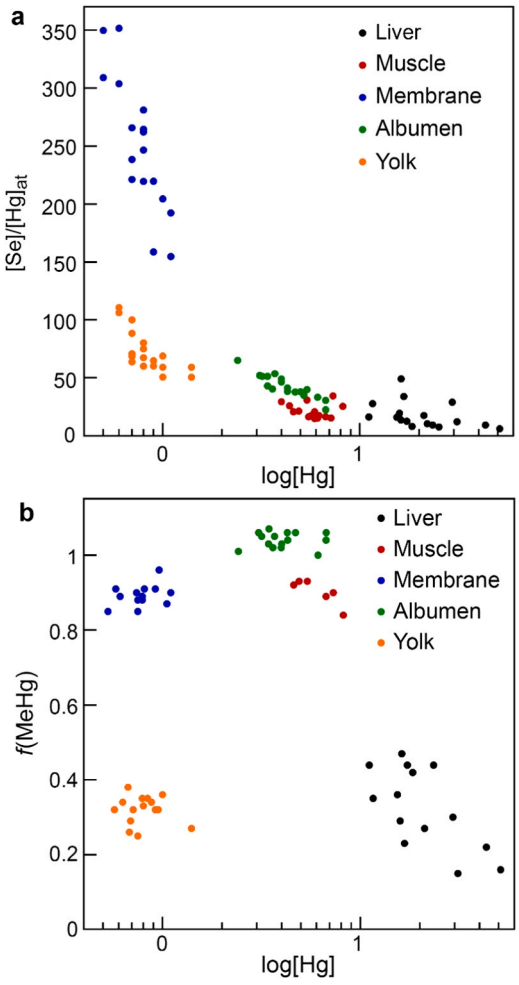

Fig. 1. Se:Hg atomic ratio (a) and fraction of MeHg from chemical analysis (b) as a function of total Hg in liver and muscles tissues, and in egg components.

as bioindicators of the circumantarctic Hg contamination confirmed that predators from the Ross Sea are more exposed to Hg than in other locations.[114].

The albumen has four times more THg than the yolk (Table S3) and weighs about twice as much when calculating the total mass of the egg. Furthermore, based on chemical measurements the albumen contains mostly MeHg (104 ± 2 %) whereas MeHg in the yolk only accounts for 32 ± 4 % of the total Hg. Thus, the amount and chemical form of Hg transferred to the chick greatly differs between the two egg components, as observed in other birds [115–117], with MeHg being the main Hg form transferred by the mother to the chick embryos [118,119]. The lack of IHg in the egg albumen can be explained by the complexation of MeHg to the thiol groups of ovalbumin, which was observed to contain more than 97 % THg in laying hens [115]. However, previous studies showed that transfer of MeHg during egg production is quantitatively minor compared to depuration into feathers during molt [5,117,120].

3.2. Coordination structure of the IHg species

Six liver tissues, out of the 18 total (Table S3), were measured by HERFD-XANES (EP04-L, EP06-L, EP10-L, EP12-L, EP15-L, EP18-L, Table S4). Data analysis showed that the six spectra are not mixtures of just two main Hg forms, a methylated (MeHg) and an inorganic (IHg) form, which is typically assumed when using chemical speciation methods as well as Hg isotope analyses [33]. This is illustrated in Fig. 2a for the HERFD-XANES spectra of EP04-L, EP06-L and EP18-L, which show that there is no isosbestic point where the three curves meet. One

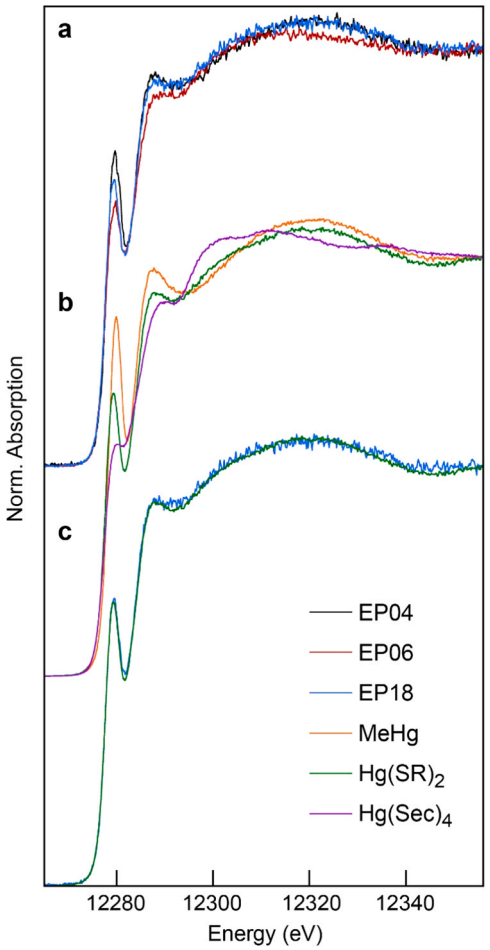

Fig. 2. (a) Hg L_3-edge HERFD-XANES spectra of three liver tissues illustrating the variability in Hg speciation. (b) HERFD-XANES reference spectra used to fit liver data. (c) Comparison of the EP18-L and $Hg(SR)_2$ spectra.

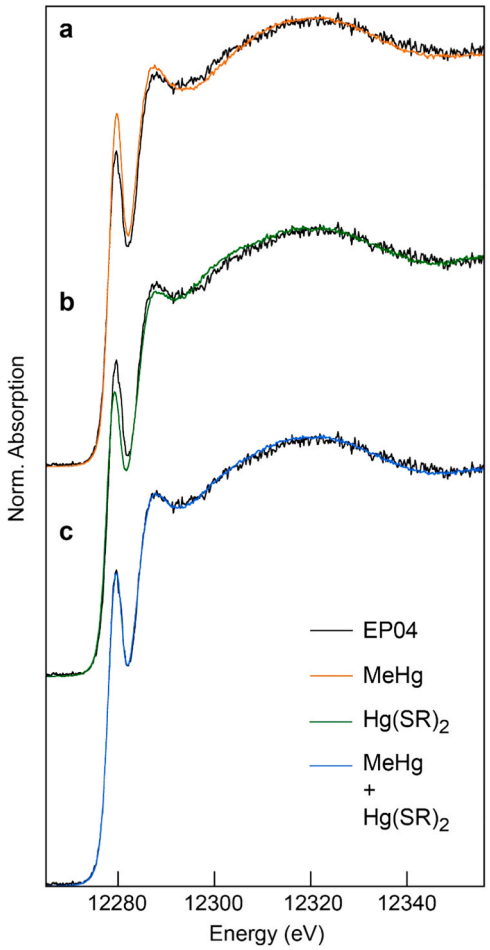

Fig. 3. Fit of the HERFD-XANES spectrum for EP04-L with MeHg (a) and Hg $(SR)_2$ (b) reference spectra ($NSS = 5.5 \times 10^{-4}$, $NSS = 4.5 \times 10^{-4}$, respectively), and with the two reference spectra ($NSS = 1.1 \times 10^{-4}$) (c).

organic (MeHg, SPOIL = 0.9) and two inorganic ($Hg(Sec)_4$, SPOIL = 1.2; and $Hg(SR)_2$, SPOIL = 1.6) coordination structures were identified by PCA and TT (Fig. 2b and S2a-c). However, the spectral reconstruction of HgSe by TT was poor (Fig. S2d). MeHgSec and $Hg(Sec)_2$ are minor (< ~10 %) complexes, if present in the tissue. The six tissues contain different molar fractions of two or three of the positively identified MeHg, $Hg(Sec)_4$ and $Hg(SR)_2$ complexes, except EP18-L which has only $Hg(SR)_2$ (Fig. 2c, Table S4). In EP04-L for example, Hg is 46 ± 10 % MeHg and 54 ± 9 % $Hg(SR)_2$, whereas EP06-L contains 59 ± 15 % Hg $(SR)_2$ and 40 ± 15 % $Hg(Sec)_4$. Linear combination fits of EP04-L and EP06-L with one Hg component are compared in Figs. 3 and 4 to the fits with two components. This modeling exercise illustrates the sensitivity of HERFD-XANES spectra to elucidate Hg coordination structures, specifically the ability to resolve the $Hg(SR)_2$ and $Hg(Sec)_4$ complexes.

The presence of the single $Hg(SR)_2$ form in EP18-L, which contains over 3.0 μg Hg/g, provides strong evidence that this complex is a biochemical demethylation product. The hypothesis that EP18-L could be an outlier and fed mainly on krill at shallower diving depth is ruled out by the Δ^{199}Hg and δ^{15}N values. EP18-L has a Δ^{199}Hg value of 1.22 ± 0.04 ‰, which aligns with the average liver value for all EPs (1.25 ± 0.11, $n = 14$, Table S5) confirming similar foraging habits between individuals in this study. Similarly, the liver δ^{15}N value (11.9 ‰) does not differ from the average value measured on the six EP analyzed by HERFD-XANES (12.3 ± 0.7 ‰). The same observation holds for the muscle tissue (δ^{15}N = 9.4 ‰ versus 9.9 ± 0.6 ‰, Table S4). Furthermore, if EP18-L was feeding on krill, we would expect a lower trophic level given the differences in trophic position between silverfish (δ^{15}N = 10.6 ± 0.3 ‰) and Antarctic and ice krill (δ^{15}N = 5.5 ± 0.4 and 6.8 ± 0.7 ‰, respectively) [47].

The fraction of $Hg(Sec)_4$ in the six livers ranges between 0 % to a maximum of 40 % in EP06-L, which also has the highest THg concentration (5.1 μg/g, Table S3). Calculation of the chemical and effective Se:THg ratios (Eq. 1) shows that EP06-L has $[Se]_{chem}$:[Hg] = 8.4 and $[Se]_{eff}$:[Hg] = 5.2. The correction to the $[Se]_{chem}$:[Hg] molar ratio to account for the bonding of the Hg atoms to four selenolate ligands is 38 %. The concentration of bioavailable Se is 9.9 μg/g (0.12 mM) for a total of 10.7 μg/g (Eq. 2), thus clearly sufficient to meet the physiological requirement of the body. Selenium is essential for male fertility in mammals [60]. SelP deficiency, in particular, alters the supply of Se to testis, leading to the production of abnormal spermatozoa [121]. No effect of Hg contamination on reproduction has been observed in penguins [6], consistent with the high level of bioavailable Se measured here.

3.3. Hg isotopic compositions

The Δ^{199}Hg value of the paired liver and muscle tissues averages to 1.28 ± 0.13 ‰ (1.05 ‰ ≤ Δ^{199}Hg ≤ 1.64 ‰, Fig. S3, Table S5) and little variation is observed as a function of %MeHg, similar to EP from the Ross Sea (1.28 ± 0.05 ‰, 1.21 ‰ ≤ Δ^{199}Hg ≤ 1.33 ‰) [33]. This value is lower than previously measured in marine fish [38,40], and is consistent with the consumption of mesopelagic prey due to the diving habits of EP, which can reach up to 500 m [122]. A Δ^{199}Hg value of 1.28 ‰ was reported for mesopelagic fish living at a median depth of

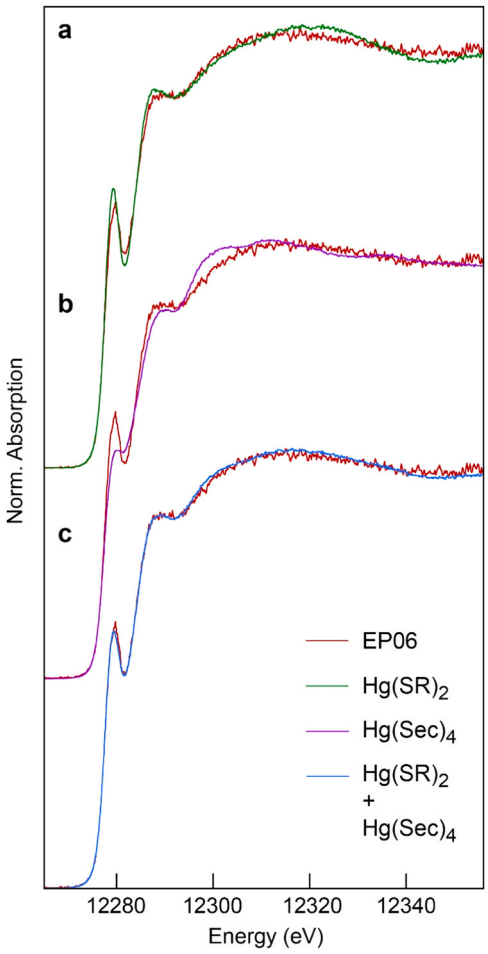

Fig. 4. Fit of the HERFD-XANES spectrum for EP06-L with $Hg(SR)_2$ (a) and $Hg(Sec)_4$ (b) reference spectra ($NSS = 5.9 \times 10^{-4}$, $NSS = 3.5 \times 10^{-4}$, respectively), and with the two reference spectra ($NSS = 1.3 \times 10^{-4}$) (c).

590 m within deep sea trenches and align with EP values in this study [42]. Thus, using Δ^{199}Hg as a bathymetric indicator of diving depth suggests that EP at Adélie Land forage at > 200 m and feed dominantly of Antarctic silverfish, as indicated by their stomach content and δ^{15}N analysis [47].

The δ^{202}Hg values exhibit large variability across livers (−0.36 to −1.81 ‰) and a large inter-tissue difference with muscles (0.40 to 0.89 ‰). The δ^{202}Hg values are linearly correlated with %MeHg (Fig. 5a), with muscle samples containing nearly exclusively MeHg and liver samples varying in the %MeHg from 15–47 %. A linear-fit of δ^{202}Hg against %MeHg yields $y = -1.98 + 2.69x$ ($R^2 = 0.93$). The first order correlation suggests that only one IHg coordination structure results from the demethylation of MeHg. This linear fit indicates that the IHg form during demethylation has a δ^{202}Hg value of −1.98 ± 0.10 ‰, which is on the order of previous $\delta^{202}Hg(Sec)_4$ measurements in giant petrels (−1.37 ± 0.06 ‰) [31] and in long-finned pilot whales (−1.56 and −1.33 ‰) [54]. The 2.7 ‰ difference in δ^{202}Hg between MeHg and IHg, which is the product-reactant isotope enrichment factor ($\varepsilon_{p/r}$), is similar to the previously reported 3.0 ‰ value in seals [123], 2.6 to 3.0 ‰ in long-finned pilot whales [53,54], and 2.2 ‰ in waterbirds [55]. The difference is much greater in giant petrels (4.1 ± 0.1 ‰) for reasons discussed previously [31].

The δ^{202}Hg - %MeHg correlation shown in Fig. 5a has also been observed previously in EP chicks [33]. However, it is noted that differences exist between the extent of demethylation and ^{202}Hg fractionation observed in adults from this study and previous studies of EP chicks [33], despite similar Hg burdens. In chicks, the minimum %MeHg was 60 % and the minimum δ^{202}Hg was −0.27 ‰ in comparison to 15 % and −1.63 ‰ (EP18-L) and 16 % and −1.81 ‰ (EP06-L) for adult EP, respectively. The reason may be either the higher demethylation ability of aged animals or that demethylation products accumulate over the lifetime of the animal, previously noted in the literature [53,61]. Therefore, demethylation pathways may be more apparent in adults compared to chicks.

The egg components have two distinct groups of δ^{202}Hg values, one of 0.70 ± 0.13 ‰ and 0.80 ± 0.05 ‰ for the albumen and membrane, and another of −1.29 ± 0.16 ‰ for the yolk (Fig. 5b). Using the %MeHg data of the egg components and δ^{202}Hg values, the isotopic variation can be described again by the simple mixing of two distinct end-member Hg coordination structures, similar to what was observed in liver and muscle tissues. The regression line ($y = -2.07 + 2.79x$, $R^2 = 0.91$) is statistically similar to that for the paired liver and muscle tissues ($y = -1.98 + 2.69x$, $R^2 = 0.93$). Thus, isotopic and chemical analysis both show that Hg is transferred as MeHg in the albumen and membrane and dominantly as IHg in the yolk. We show below that the nature of the IHg form can be inferred from the calculation of the species-specific δ^{202}Hg values.

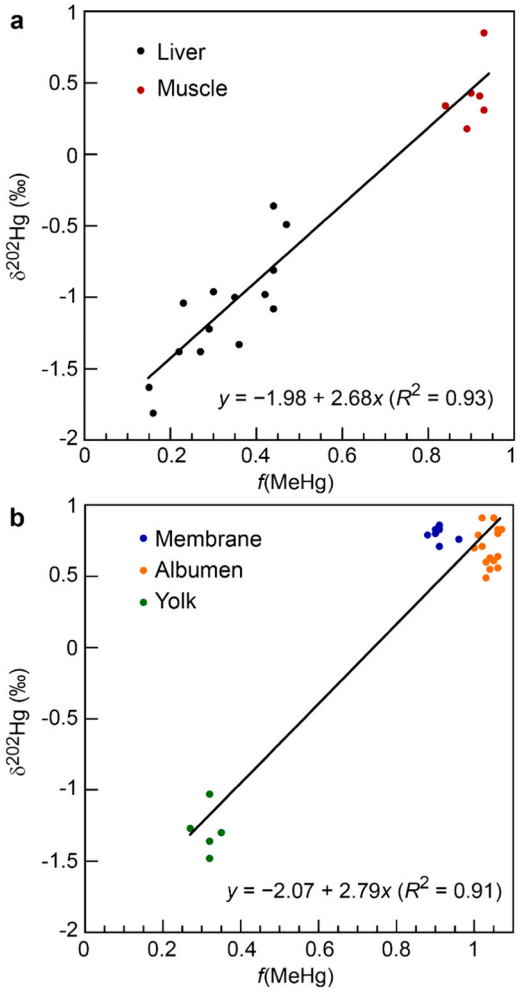

Fig. 5. Relationship between the δ^{202}Hg value of total mercury (i.e., species-averaged) and the fraction of MeHg determined by chemical analysis (a) in liver and muscle tissues, and (b) in egg components. Linear fit of plot (a) $y = -1.98(10) + 2.68(18)x$ ($R^2 = 0.93$, $p < 10^{-5}$), (b) $y = -2.07(16) + 2.79(18)x$ ($R^2 = 0.91$, $p < 10^{-5}$).

3.4. Species-specific δ^{202}Hg values

While the Hg isotope values indicate MeHg demethylation results in the formation of $Hg(Sec)_4$, the HERFD-XANES spectra indicate the presence of $Hg(SR)_2$. To account for this discrepancy, we calculated the species-specific δ^{202}Hg values for the two IHg forms ($Hg(Sec)_4$ and $Hg(SR)_2$) and MeHg. The δ^{202}Hg value measured on a liver tissue (l) is the weighted sum of the $\delta^{202}Sp_i$ value of each chemical form (i) in it [31].

$$\delta^{202}Hg_l = \sum f(Sp_i)_l \times \delta^{202}Sp_i \quad (3)$$

The species-specific δ^{202}MeHg, $\delta^{202}Hg(SR)_2$, and $\delta^{202}Hg(Sec)_4$ values can be obtained in principle by inverting Eq. 3 for the six liver tissues using linear algebra [31,54]. The optimal solution of the six equations considering three unknowns is $\delta^{202}MeHg = 0.10 \pm 0.25$ ‰, $\delta^{202}IHg_1 = -1.87 \pm 0.50$ ‰, and $\delta^{202}IHg_2 = -1.61 \pm 0.13$ ‰. The inverse problem is ill-posed, however, when three δ^{202}Hg values are optimized since the relationship between δ^{202}Hg and f(MeHg) is linear (Fig. 5a). Solving the linear system with two unknows yields $\delta^{202}MeHg = 0.24 \pm 0.10$ ‰ and $\delta^{202}IHg = -1.73 \pm 0.04$ ‰. The δ^{202}IHg value is logically in between $\delta^{202}IHg_1$ and $\delta^{202}IHg_2$. Although this solution is mathematically more robust, it does not account for the experimental values of EP06-L (-1.81 ± 0.04 ‰) and EP18-L (-1.63 ± 0.05 ‰), because they are outside the average value and standard deviation for livers ($\delta^{202}IHg = -1.73 \pm 0.04$ ‰). Thus, the -1.73 ± 0.04 ‰ value is likely a weighted average of two distinct $\delta^{202}Hg(Sec)_4$ and $\delta^{202}Hg(SR)_2$ values. The two δ^{202}IHg values are difficult to distinguish by mathematical inversion since they are aligned with δ^{202}MeHg on the δ^{202}Hg versus %MeHg graph (Fig. 5a).

Rather than solving the system of linear equations, a third approach was used that leverages the experimental δ^{202}Hg value of EP18-L for $\delta^{202}Hg(SR)_2$ (-1.63 ± 0.05 ‰), since only $Hg(SR)_2$ is detected by HERFD-XANES in this tissue (Fig. 2c, Table S4). As for $\delta^{202}Hg(Sec)_4$, its value can be obtained from the $y = -1.98 \pm 0.10$ ‰ intercept of the linear fit of the δ^{202}Hg versus %MeHg data (Fig. 5a). The average δ^{202}MeHg value obtained by this approach is 0.26 ± 0.21 ‰ and is within the uncertainty range of the values obtained by the two mathematical inversions (0.10 ± 0.25 ‰ and 0.24 ± 0.10 ‰).

The agreement of species-specific δ^{202}Hg values calculated from the three procedures can be verified *a posteriori* by recalculating the experimental species-averaged $\delta^{202}Hg_l$ values using the established $\delta^{202}Sp_i$ values and $f(Sp_i)_l$ determined by HERFD-XANES. Fig. 6 shows excellent agreement between $\delta^{202}Hg_{l,calc}$ and $\delta^{202}Hg_{l,exp}$ for the three procedures described previously ($R^2 = 0.98$–0.99). However, the three regression lines differ in their slopes. The three-variable and two-variable inversion schemes have slopes of 0.79 ± 0.06 and 0.90 ± 0.05, respectively, whereas the third scheme gives a slope near unity (1.01 ± 0.06). Therefore, we selected to use the third scheme for the final species-specific values of $\delta^{202}MeHg = 0.26 \pm 0.21$ ‰, $\delta^{202}Hg(SR)_2 = -1.63 \pm 0.20$ ‰, and $\delta^{202}Hg(Sec)_4 = -1.98 \pm 0.10$ ‰, which are rounded to $\delta^{202}MeHg = 0.3 \pm 0.2$ ‰, $\delta^{202}Hg(SR)_2 = -1.6 \pm 0.2$ ‰, and $\delta^{202}Hg(Sec)_4 = -2.0 \pm 0.1$ ‰. Note the standard deviation of δ^{202}MeHg and $\delta^{202}Hg(SR)_2$ is twice that of $\delta^{202}Hg(Sec)_4$. The higher variability of δ^{202}MeHg and $\delta^{202}Hg(SR)_2$ may reflect the large range of thiolate biomolecules capable of forming linear MeHgCys and CysHgCys complexes in the cell. The number of biomolecules likely to form a $Hg(Sec)_4$ complex is more restricted. Today, there are only two candidate species, SelP [58] and selenoneine [124]. SelP contains multiple Sec residues, a tetrahedral binding site, and was shown to be co-eluted with Hg in double affinity chromatography [58]. Density functional theory calculations showed that selenoneine also can form a tetrahedral complex with Hg despite containing only one Sec residue (Fig. S3 in ref. [58]), but its co-elution with Hg remains undocumented.

The form of IHg in the yolk, which is unknown, can be inferred from the average %MeHg value (32 %), the three species-specific δ^{202}IHg values determined from liver and muscle measurements, and the $\delta^{202}Hg_{exp}$ value (-1.29 ± 0.16 ‰, all species) (Table S3). Solving Eq. 3 gives $\delta^{202}Hg_{calc}$ of -1.02 ‰ when using δ^{202}MeHg (0.26 ‰) and $\delta^{202}Hg(SR)_2$ (-1.63 ‰) values, and a $\delta^{202}Hg_{calc}$ of -1.26 ‰ when using δ^{202}MeHg and $\delta^{202}Hg(Sec)_4$ (-1.98 ‰) values. Therefore, we propose the IHg form in the yolk is $Hg(Sec)_4$. The agreement between the calculated (-1.26 ‰) and the experimental (-1.29 ‰) values provides confidence in the robustness of the cross-analysis of the independent isotopic and spectroscopic data by mathematical inversion [31,54].

Inability of an embryo to synthesize selenoproteins leads to its death [125] and maternal-fetal Se supply is ensured partly by the transfer of SelP in the epithelial cells of the visceral yolk sac through pinocytosis at the beginning of incubation [126]. This mechanisms may be how $Hg(Sec)_4$ ended up, at least partly, in chick yolk. After several hours to few days of development of the fertilized egg, this mechanism ceases [126] and is replaced by the biosynthesis of SelP by the yolk cell nucleus [127].

4. Conclusion

The results presented herein shed light on the inorganic forms of Hg in a mesopredator seabird feeding at lower trophic level or foraging in less contaminated ecosystem than most large flying seabirds and waterbirds. Two main differences with our previous Hg demethylation studies using HERFD-XANES on giant petrels [57] and the Clark's grebe [58] are the lack of HgSe and the large amounts of $Hg(SR)_2$ mixed with $Hg(Sec)_4$ in EP. Production of HgSe seems to be linked to the total Hg concentration, and therefore to the trophic level and foraging habitat of the animal. In giant petrels, which are apex predators and marine scavengers, the liver contained between 90–100 % (HgSe) ($n = 5$) and had Hg concentrations ranging from 170 to 1499 μg/g. The Clark's grebe, which was from a contaminated site in the United States and showed a liver Hg concentration of 43 μg/g, had predominantly Hg $(Sec)_4$ (86 %) in its liver and minor nanoparticulate $Hg_x(Se,Sec)_y$/HgSe ($n = 1$). In contrast, this study demonstrated that EP livers had total Hg content ≤ 5 μg/g and 0–40 % of the IHg present was $Hg(Sec)_4$ and 42–100 % was $Hg(SR)_2$ ($n = 5$). This work indicates that IHg coordination structure stemming from MeHg demethylation can vary dramatically across avian species.

While $Hg(Sec)_4$ is clearly a demethylation product [57,58], the origin of $Hg(SR)_2$ is not well understood. At present, only bacteria and archaea can demethylate MeHg biotically to $Hg(SR)_2$ [128]. Demethylation by intestinal microorganisms, such as those isolated from yellowfin tuna [129], is unlikely because bacteria have significantly lower product–reactant isotopic enrichment factor ($\varepsilon_{Hg(SR)2/MeHg} = -0.4 \pm 0.2$ ‰) [130] than that observed here (-1.9 ± 0.2 ‰). Similarly, a dietary source for $Hg(SR)_2$ can be refuted on the basis of the Δ^{199}Hg and δ^{15}N isotopic values and analysis of stomach contents, which show that EP prey primarily on fish in Adélie Land. Therefore, $Hg(SR)_2$ is most likely a byproduct of the intracellular demethylation of MeHg. In *mer*-mediated bacterial demethylation, MeHg is converted to CH_4 and inorganic Hg(II) by the organomercurial lyase MerB and this enzyme binds MeHg to two Cys residues, weakening and cleaving the Hg-C bond with subsequent formation of CH_4 [131,132]. The resulting Hg complex is $Hg(SR)_2$. A similar biochemical mechanism for MeHg degradation may exist in multicellular organisms, but this remains unknown. Further research is needed to understand why thiol ligands are not exchanged for Se ligands, as on model compounds [70–73], to form $Hg(Sec)_4$, as there is no Se deficiency in the liver.

Environmental implication

In the global environment, and the Antarctic in particular, MeHg is a toxic species that organisms have to deal with. The dogma is that it is selenium which reduces MeHg toxicity by demethylation. In another polar bird from the same area, the Antarctic skua, Hg has a significant negative effect on reproduction and demography [133], which seems to be linked to low levels of selenium in this species [134]. The new

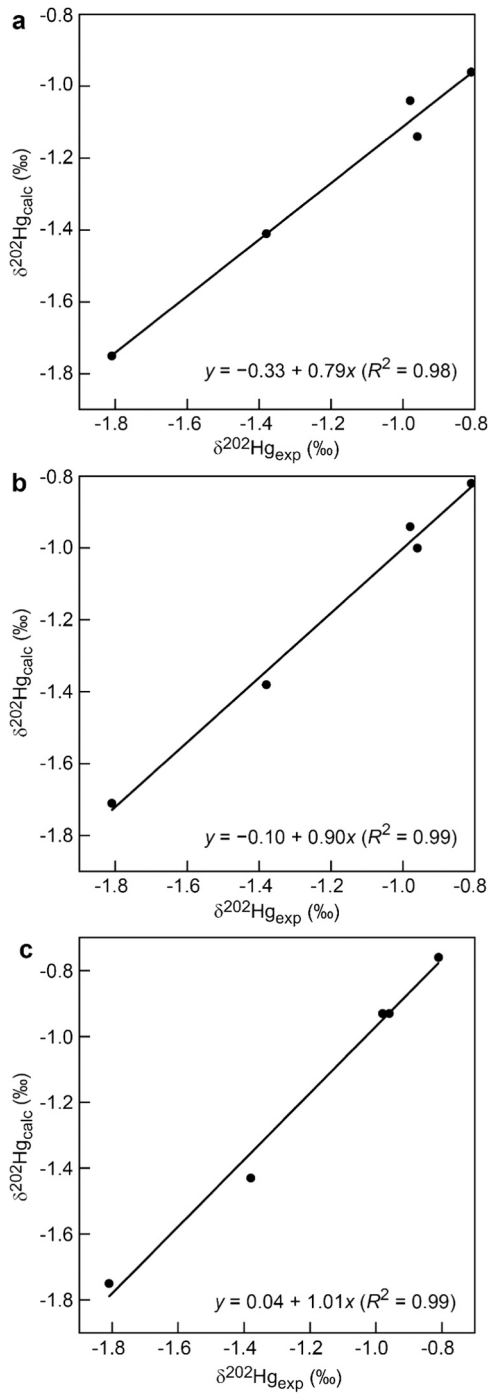

Fig. 6. Calculated versus measured species-averaged values of $\delta^{202}Hg$ ($\delta^{202}Hg_{calc}$ versus $\delta^{202}Hg_{exp}$, respectively). (a) $\delta^{202}Hg_{calc}$ calculated with $\delta^{202}MeHg = 0.10$ ‰, $\delta^{202}IHg_1 = -1.87$ ‰, and $\delta^{202}IHg_2 = -1.61$ ‰ obtained by solving Eq. 3 with three unknows. (b) $\delta^{202}Hg_{calc}$ calculated with $\delta^{202}MeHg = 0.24$ ‰ and $\delta^{202}IHg = -1.73$ ‰ obtained by solving Eq. 3 with two unknows. (c) $\delta^{202}Hg_{calc}$ calculated with $\delta^{202}MeHg = 0.26$ ‰, $\delta^{202}Hg(SR)_2 = -1.63$ ‰, and $\delta^{202}Hg(Sec)_4 = -1.98$ ‰.

detoxification pathway using sulfur could enable predators to demethylate MeHg even when selenium supply is low.

CRediT authorship contribution statement

Alain Manceau: Writing – original draft, Methodology, Investigation, Formal analysis, Conceptualization. **Brett A. Poulin:** Writing – review & editing, Funding acquisition. **Yves Cherel:** Writing – review & editing, Conceptualization. **Etienne Richy:** Methodology. **Pieter Glatzel:** Methodology. **Sarah E. Janssen:** Writing – review & editing, Methodology, Formal analysis. **Paco Bustamante:** Writing – review & editing, Methodology, Formal analysis, Conceptualization.

Declaration of Competing Interest

The authors declare that they have no known competing financial interests or personal relationships that could have appeared to influence the work reported in this paper.

Acknowledgments

The authors thank fieldworkers who collected tissue samples during the Austral winter. Fieldwork was approved by the Conseil des Programmes Scientifiques et Technologies Polaires of the Institut Polaire Français Paul Emile Victor (IPEV), and procedures were approved by the Animal Ethics Committee of IPEV. We are grateful to Carine Churlaud and Maud Brault-Favrou from the Plateforme Analyses Elémentaires (LIENSs) for her support during Hg and Se analyses, and Gaël Guillou from the Plateforme Analyses Isotopiques (LIENSs) for running stable isotope measurements. We also acknowledge Michael Tate and Grace Armstrong for the preparation and analysis of Hg isotope samples. The authors acknowledge Julien Vasseur for the photo of the emperor penguin used in the table of contents (TOC) art. Five anonymous reviewers are acknowledged for constructive comments on the manuscript. PB is an honorary member of the Institut Universitaire de France (IUF). The present work was supported financially and logistically by IPEV (Programme N°109, C. Barbraud) and the Terres Australes et Antarctiques Françaises, and by a grant from the National Science Foundation to BAP (EAR-2143243). The AMA and IRMS at LIENSs were acquired with CPER (Contrat de Projet Etat-Région) and FEDER (Fonds Européen de Développement Régional) funds. This work was supported by the U.S. Geological Survey Environmental Health-Toxic Substances Hydrology and Contaminant Biology Programs. Any use of trade, firm, or product names is for descriptive purposes only and does not imply endorsement by the U.S. Government.

Appendix A. Supporting information

Supplementary data associated with this article can be found in the online version at doi:10.1016/j.jhazmat.2024.136499.

Data availability

Data are in the Supporting Information.

References

[1] Norheim, G., 1987. Levels and interactions of heavy-metals in sea birds from Svalbard and the Antarctic. Environ Pollut 47, 83–94.
[2] Szefer, P., Czarnowski, W., Pempkowiak, J., Holm, E., 1993. Mercury and major essential elements in seals, penguins, and other representative fauna of the Antarctic. Arch Environ Con Tox 25, 422–427.
[3] Blevin, P., Carravieri, A., Jaeger, A., Chastel, O., Bustamante, P., Cherel, Y., 2013. Wide range of mercury contamination in chicks of southern ocean seabirds. Plos One 8 (e54508).
[4] Brasso, R., Chiaradia, A., Polito, M., Rey, A., Emslie, S., 2015. A comprehensive assessment of mercury exposure in penguin populations throughout the Southern Hemisphere: using trophic calculations to identify sources of population-level variation. Mar Pollut Bull 97, 408–418.
[5] Albert, C., Renedo, M., Bustamante, P., Fort, J., 2019. Using blood and feathers to investigate large-scale Hg contamination in Arctic seabirds: a review. Environ Res 177 (108588).
[6] Ibanez, A., Mills, W.F., Bustamante, P., Morales, L.M., Torres, D.S., D'Astek, B., Mariano-Jelicich, R., Phillips, R.A., Montalti, D., 2024. Deleterious effects of mercury contamination on immunocompetence, liver function and egg volume in an antarctic seabird. Chemosphere 346 (140630).

[7] Gimeno, M., et al., 2024. Assessing mercury contamination in Southern hemisphere marine ecosystems: the role of penguins as effective bioindicators. Environ Pollut 343 (123159).

[8] Honda, K., Yamamoto, Y., Hidaka, H., Tatsukawa, R., 1986. Heavy metal accumulation in Adelie penguin. *Pygoscelis adeliae*, their Var Reprod Process, Mer Natl Inst Polar Res Spec 40, 443–453.

[9] Honda, Yamamoto, K., Kato, H., Tatsukawa, R., 1987. Heavy metal accumulation and their recent changes in southern minke whales *Balaenoptera acutorostrata*. Arch Environ Contam Toxicol 16, 209–216.

[10] Yamamoto, Y., Honda, K., Hidaka, H., Tatsukawa, R., 1987. Tissue distribution of heavy-metals in weddell seals (*Leptonychotes weddellii*). Mar Pollut Bull 18, 164–169.

[11] Marumoto, M., Sakamoto, M., Nakamura, M., Marumoto, K., Tsuruta, S., 2022. Organ-specific accumulation of selenium and mercury in Indo-Pacific bottlenose dolphins (*Tursiops aduncus*). Acta Vet Scand 64 (1).

[12] Sakamoto, M., Itai, T., Yasutake, A., Iwasaki, T., Yasunaga, G., Fujise, Y., Nakamura, M., Murata, K., Chan, H.M., Domingo, J.L., Marumoto, M., 2015. Mercury speciation and selenium in toothed-whale muscles. Environ Res 143, 55–61.

[13] McCormack, M.A., Jackson, B.P., Dutton, J., 2020. Relationship between mercury and selenium concentrations in tissues from stranded odontocetes in the northern Gulf of Mexico. Sci Tot Environ 749 (141350).

[14] Martinez-López, E., Peñalver, J., Lara, L., García-Fernández, A.J., 2019. Hg and Se in organs of three cetacean species from the murcia coastline (Mediterranean Sea). Bull Environ Contam Tox 103, 521–527.

[15] Lailson-Brito, J., Cruz, R., Dorneles, P.R., Andrade, L., Azevedo, A.D., Fragoso, A. B., Vidal, L.G., Costa, M.B., Bisi, T.L., Almeida, R., Carvalho, D.P., Bastos, W.R., Malm, O., 2012. Mercury-selenium relationships in liver of Guiana dolphin: the possible role of Kupffer cells in the detoxification process by tiemannite formation. Plos One 7 (e42162).

[16] Cardellicchio, N., Decataldo, A., Di Leo, A., Misino, A., 2002. Accumulation and tissue distribution of mercury and selenium in striped dolphins (Stenella coeruleoalba) from the Mediterranean Sea (southern Italy). Environ Poll 116, 265–271.

[17] Endo, T., Haraguchi, K., Sakata, M., 2002. Mercury and selenium concentrations in the internal organs of toothed whales and dolphins marketed for human consumption in Japan. Sci Tot Environ 300, 15–22.

[18] Caurant, F., Navarro, M., Amiard, J., 1996. Mercury in pilot whales: possible limits to the detoxification process. Sci Tot Environ 186, 95–104.

[19] Ralston, N.V.C., Raymond, L.J., 2010. Dietary selenium's protective effects against methylmercury toxicity. Toxicology 278, 112–123.

[20] Ralston, N.V.C., Raymond, L.J., 2018. Mercury's neurotoxicity is characterized by its disruption of selenium biochemistry. BBA-Gen Sub 1862, 2405–2416.

[21] Capelli, R., Drava, G., De Pellegrini, R., Minganti, V., Poggi, R., 2000. Study of trace elements in organs and tissues of striped dolphins (*Stenella coeruleoalba*) found dead along the Ligurian coasts (Italy). Adv Environ Res 4, 31–43.

[22] Peterson, S.A., Ralston, N.V.C., Peck, D.V., Sickle, J.Van, Robertson, J.D., Spate, V.L., Morris, J.S., 2009. How might selenium moderate the toxic effects of mercury in stream fish of the western US? Environ Sci Technol 43, 3919–3925.

[23] Kaneko, J.J., Ralston, N.V.C., 2007. Selenium and mercury in pelagic fish in the Central North Pacific near Hawaii. Biol Trace Elem Res 119, 242–254.

[24] Adams, W.J., Duguay, A., 2024. Selenium–mercury interactions and relationship to aquatic toxicity: a review. Integr Environ Assess Manag (in press.).

[25] James, A., Dolgova, N., Nehzati, S., Korbas, M., Cotelesage, J., Sokaras, D., Kroll, T., O'Donoghue, J., Watson, G., Myers, G., Pickering, I., George, G., 2022. Molecular fates of organometallic mercury in human brain. ACS Chem Neurosci 13, 1756–1768.

[26] Zheng, W., Xie, Z.Q., Bergquist, B.A., 2015. Mercury stable isotopes in ornithogenic deposits as tracers of historical cycling of mercury in Ross Sea, Antarctica. Environ Sci Technol 49, 7623–7632.

[27] Renedo, M., Amouroux, D., Duval, B., Carravieri, A., Tessier, E., Barre, J., Berail, S., Pedrero, Z., Cherel, Y., Bustamante, P., 2018. Seabird tissues as efficient biomonitoring tools for Hg isotopic investigations: implications of using blood and feathers from chicks and adults. Environ Sci Technol 52, 4227–4234.

[28] Renedo, M., Amouroux, D., Pedrero, Z., Bustamante, P., Cherel, Y., 2018. Identification of sources and bioaccumulation pathways of MeHg in subantarctic penguins: a stable isotopic investigation. Sci Rep 8 (8865).

[29] Renedo, M., Bustamante, P., Cherel, Y., Pedrero, Z., Tessier, E., Amouroux, D., 2020. A "seabird-eye" on mercury stable isotopes and cycling in the Southern Ocean. Sci Tot Environ 742 (140499).

[30] Renedo, M., Pedrero, Z., Amouroux, D., Cherel, Y., Bustamante, P., 2021. Mercury isotopes of key tissues document mercury metabolic processes in seabirds. Chemosphere 263 (n° 127777).

[31] Manceau, A., Brossier, R., Janssen, S.E., Rosera, T.J., Krabbenhoft, D.P., Cherel, Y., Bustamante, P., Poulin, B.A., 2021. Mercury isotope fractionation by internal demethylation and biomineralization reactions in seabirds: implications for environmental mercury science. Environ Sci Technol 55, 13942–13952.

[32] Le Croizier, G., Sonke, J.E., Lorrain, A., Renedo, M., Hoyos-Padilla, M., Santana-Morales, O., Meyer, L., Huveneers, C., Butcher, P., Amezcua-Martinez, F., Point, D., 2022. Foraging plasticity diversifies mercury exposure sources and bioaccumulation patterns in the world's largest predatory fish. J Hazard Mater 425 (127956).

[33] Jung, S.B., Besnard, L., Li, M.L., Reinfelder, J., Kim, E., Kwon, S.Y., Kim, J.H., 2024. Interspecific variations in the internal mercury isotope dynamics of Antarctic penguins: implications for biomonitoring. Environ Sci Technol 58, 6349–6358.

[34] Bergquist, B.A., Blum, J.D., 2007. Mass-dependent and -independent fractionation of Hg isotopes by photoreduction in aquatic systems. Science 318, 417–420.

[35] Chandan, P., Ghosh, S., Bergquist, B.A., 2015. Mercury isotope fractionation during aqueous photoreduction of monomethylmercury in the presence of dissolved organic matter. Environ Sci Technol 49, 259–267.

[36] Rose, C., Ghosh, S., Blum, J.D., Bergquist, B.A., 2015. Effects of ultraviolet radiation on mercury isotope fractionation during photo-reduction for inorganic and organic mercury species. Chem Geol 405, 102–111.

[37] Tsui, M.T.K., Blum, J.D., Kwon, S.Y., 2020. Review of stable mercury isotopes in ecology and biogeochemistry. Sci Tot Environ 716 (135386).

[38] Blum, J.D., Popp, B.N., Drazen, J.C., Choy, C.A., Johnson, M.W., 2013. Methylmercury production below the mixed layer in the North Pacific Ocean. Nat Geosci 6, 879–884.

[39] Sackett, D.K., Drazen, J.C., Popp, B.N., Choy, C.A., Blum, J.D., Johnson, M.W., 2017. Carbon, nitrogen, and mercury isotope evidence for the biogeochemical history of mercury in Hawaiian Marine Bottomfish. Environ Sci Technol 51, 13976–13984.

[40] Madigan, D.J., Li, M.L., Yin, R.S., Baumann, H., Snodgrass, O., Dewar, H., Krabbenhoft, D.P., Baumann, Z., Fisher, N.S., Balcom, P., Sunderland, E.M., 2018. Mercury stable isotopes reveal influence of foraging depth on mercury concentrations and growth in Pacific Bluefin Tuna. Environ Sci Technol 52, 6256–6264.

[41] Masbou, J., Sonke, J.E., Amouroux, D., Guillou, G., Becker, P.R., Point, D., 2018. Hg-stable isotope variations in marine top predators of the western Arctic Ocean. ACS Earth Space Chem 2, 479–490.

[42] Blum, J.D., Drazen, J.C., Johnson, M.W., Popp, B.N., Motta, L.C., Jamieson, A.J., 2020. Mercury isotopes identify near-surface marine mercury in deep-sea trench biota. Proc Natl Acad Sci USA 117, 29292–29298.

[43] Le Croizier, G., Lorrain, A., Sonke, J.E., Hoyos-Padilla, E.M., Galvan-Magana, F., Santana-Morales, O., Aquino-Baleyto, M., Becerril-Garcia, E.E., Muntaner-Lopez, G., Ketchum, J., Block, B., Carlisle, A., Jorgensen, S.J., Besnard, L., Jung, A., Schaal, G., Point, D., 2020. The twilight zone as a major foraging habitat and mercury source for the great white shark. Environ Sci Technol 54, 15872–15882.

[44] Le Croizier, G., Lorrain, A., Sonke, J., Jaquemet, S., Schaal, G., Renedo, M., Besnard, L., Cherel, Y., Point, D., 2020. Mercury isotopes as tracers of ecology and metabolism in two sympatric shark species. Environ Pollut 265 (114931).

[45] Besnard, L., Le Croizier, G., Galván-Magaña, F., Point, D., Kraffe, E., Ketchum, J., Rincon, R., Schaal, G., 2021. Foraging depth depicts resource partitioning and contamination level in a pelagic shark assemblage: Insights from mercury stable isotopes. Environ Pollut 283 (117066).

[46] Cherel, Y., Kooyman, G.L., 1998. Food of emperor penguins (*Aptenodytes forsteri*) in the western Ross Sea, Antarctica. Mar Biol 130, 335–344.

[47] Cherel, Y., 2008. Isotopic niches of emperor and Adélie penguins in Adélie Land, Antarctica. Mar Biol 154, 813–821.

[48] Hong, S., Gal, J., Lee, B., Son, W., Jung, J., La, H., Shin, K., Kim, J., Ha, S., 2021. Regional differences in the diets of adelie and emperor penguins in the Ross Sea, Antarctica. Animals 11 (2681).

[49] Minagawa, M., Wada, E., 1984. Stepwise entichment of ^{15}N along food-chains - Further evidence and the relation between $\delta^{15}N$ and animal age. Geochim Cosm Acta 48, 1135–1140.

[50] Vanderklift, M.A., Ponsard, S., 2003. Sources of variation in consumer-diet $\delta^{15}N$ enrichment: a meta-analysis. Oecologia 136, 169–182.

[51] dos Santos, I., Paiva, V.H., Norte, A.C., Churlaud, C., Ceia, F.R., Pais de Faria, J., Pereira, J.M., Cerveira, L.R., Laranjeiro, M.I., Verissimo, S.N., Ramos, J.A., Bustamante, P., 2024. Assessing the impacts of trace element contamination on the physiological and health of seabirds breeding along the western and southern coasts of Portugal. Environ Pollut 358 (124528).

[52] Lemesle, P., Jouanneau, W., Cherel, Y., Legroux, N., Ward, A., Bustamante, P., Chastel, O., 2024. Mercury exposure and trophic ecology of urban nesting black-legged kittiwakes from France. Chemosphere 363 (142813). https://www.sciencedirect.com/science/article/pii/S0045653524017077.

[53] Li, M.L., Juang, C.A., Ewald, J.D., Yin, R.S., Mikkelsen, B., Krabbenhoft, D.P., Balcom, P.H., Dassuncao, C., Sunderland, E.M., 2020. Selenium and stable mercury isotopes provide new insights into mercury toxicokinetics in pilot whales. Sci Tot Environ 710 (136325).

[54] Manceau, A., Brossier, R., Poulin, B.A., 2021. Chemical forms of mercury in pilot whales determined from species-averaged mercury isotope signatures. ACS Earth Space Chem 5, 1591–1599.

[55] Poulin, B.A., Janssen, S.E., Rosera, T.J., Krabbenhoft, D.P., Eagles-Smith, C.A., Ackerman, J.T., Stewart, A.R., Kim, E., Baumann, Z., Kim, J.H., Manceau, A., 2021. Isotope fractionation from in vivo methylmercury detoxification in waterbirds. ACS Earth Space Chem 5, 990–997.

[56] Li, M.L., Kwon, Y., Poulin, A., Tsui, M.T.K., Motta, C., Cho, M., 2022. Internal dynamics and metabolism of mercury in biota: a review of insights from mercury stable isotopes. Environ Sci Technol 56, 9182–9195.

[57] Manceau, A., Gaillot, A.C., Glatzel, P., Cherel, Y., Bustamante, P., 2021. In vivo formation of HgSe nanoparticles and Hg-tetraselenolate complex from methylmercury in seabird – Implications for the Hg-Se antagonism. Environ Sci Technol 55, 1515–1526.

[58] Manceau, A., Bourdineaud, J.P., Oliveira, R.B., Sarrazin, S.L.F., Krabbenhoft, D. P., Eagles-Smith, C.A., Ackerman, J.T., Stewart, A.R., Ward-Deitrich, C., Busto, M. E.D., Goenaga-Infante, H., Wack, A., Retegan, M., Detlefs, B., Glatzel, P., Bustamante, P., Nagy, K.L., Poulin, B.A., 2021. Demethylation of methylmercury in bird, fish, and earthworm. Environ Sci Technol 55, 1527–1534.

[59] Burk, R.F., Hill, K.E., 2015. In: Bowman, B.A., Stover, P.J. (Eds.), Regulation of Selenium Metabolism and Transport. Annu. Rev. Nutr, pp. 109–134.
[60] Burk, R.F., Hill, K.E., 2009. Selenoprotein P-Expression, functions, and roles in mammals. BBA-Gen Subj 1790, 1441–1447.
[61] Gajdosechova, Z., Lawan, M.M., Urgast, D.S., Raab, A., Scheckel, K.G., Lombi, E., Kopittke, P.M., Loeschner, K., Larsen, E.H., Woods, G., Brownlow, A., Read, F.L., Feldmann, J., Krupp, E.M., 2016. In vivo formation of natural HgSe nanoparticles in the liver and brain of pilot whales. Sci Rep 6 (34361).
[62] Nigro, M., Leonzio, C., 1996. Intracellular storage of mercury and selenium in different marine vertebrates. Mar Ecol Prog Ser 135, 137–143.
[63] Rawson, A., Bradley, J.P., Teetsov, A., RICE, S.B., Haller, E.M., Patton, G.W., 1995. A role of airborne-particulates in high mercury levels of some cetaceans. Ecotoxicol Environ Saf 30, 309–314.
[64] Arai, T., Ikemoto, T., Hokura, A., Terada, Y., Kunito, T., Tanabe, S., Nakai, I., 2004. Chemical forms of mercury and cadmium accumulated in marine mammals and seabirds as determined by XAFS analysis. Environ Sci Technol 38, 6468–6474.
[65] Huggins, F.E., Raverty, S.A., Nielsen, O.S., Sharp, N.E., Robertson, J.D., Ralston, N.V.C., 2009. An XAFS investigation of mercury and selenium in Beluga whale tissues. Environ Bioindic 4, 291–302.
[66] Nakazawa, E., Ikemoto, T., Hokura, A., Terada, Y., Kunito, T., Tanabe, S., Nakai, I., 2011. The presence of mercury selenide in various tissues of the striped dolphin: evidence from μ-XRF-XRD and XAFS analyses. Metallomics 3, 719–725.
[67] Ji, X.M., Yang, L., Wu, F.X., Yao, L.L., Yu, B., Liu, X., Yin, Y., Hu, L., Qu, G., Fu, J., Yang, R., Wang, X., Shi, J., Jiang, G., 2022. Identification of mercury-containing nanoparticles in the liver and muscle of cetaceans. J Hazard Mater 424 (127759).
[68] von Hellfeld, R., Gade, C., Doeschate, M. ten, Davison, N.J., Brownlow, A., Mbadugha, L., Hastings, A., Paton, G., 2024. High resolution visualisation of tiemannite microparticles, essential in the detoxification process of mercury in marine mammals. Environ Pollut 342 (123027).
[69] Paton, L., Moro, T.T., Lockwood, T., Maranhao, T.D., Gössler, G., Clases, D., Feldmann, J., 2024. AF_4-MALS-SP ICP-ToF-MS analysis gives insight into nature of HgSe nanoparticles formed by cetaceans. Environ Sci Nano 11, 1883–1890.
[70] Sugiura, Y., Tamai, Y., Tanaka, H., 1978. Selenium protection against toxicity - High binding affinity of methylmercury by selenium-containing ligands in comparison with sulfur-containing ligands. Bioinorg Chem 9, 167–180.
[71] Khan, M.A.K., Wang, F.Y., 2010. Chemical demethylation of methylmercury by selenoamino acids. Chem Res Toxicol 23, 1202–1206.
[72] Melnick, J.G., Yurkerwich, K., Parkin, G., 2010. On the chalcogenophilicity of mercury: evidence for a strong Hg-Se bond in [Tm^{But}]HgSePh and its relevance to the toxicity of mercury. J Am Chem Soc 132, 647–655.
[73] de Maria, M.B., Tesauro, D., Prencipe, F., Saviano, M., Messori, L., Enjalbal, C., Lobinski, R., Ronga, L., 2023. Disclosing the preferential mercury chelation by SeCys containing peptides over their Cys analogues. Inorg Chem 62, 14980–14990.
[74] Bloom, N.S., 1992. On the chemical form of mercury in eddible fish and marine invertebrate tissue. Can J Fish Aquat Sci 49, 1010–1017.
[75] Harris, H.H., Pickering, I.J., George, G.N., 2003. The chemical form of mercury in fish. Science 301, 1203.
[76] Kuwabara, J.S., Arai, Y., Topping, B.R., Pickering, I.J., George, G.N., 2007. Mercury speciation in piscivorous fish from mining-impacted reservoirs. Environ Sci Technol 41, 2745–2749.
[77] Minet, A., Manceau, A., Valada-Mennuni, A., Brault-Favrou, M., Churlaud, C., Fort, J., Nguyen, T.C., Spitz, J., Bustamante, P., Lacoue-Labarthe, T., 2021. Mercury in the tissues of five cephalopods species: first data on the nervous system. Sci Tot Environ 759 (143907).
[78] Sontag, P.T., Steinberg, D.K., Reinfelder, J.R., 2019. Patterns of total mercury and methylmercury bioaccumulation in Antarctic krill (Euphausia superba) along the West Antarctic Peninsula. Sci Tot Environ 688, 174–183.
[79] Seco, J., Xavier, J., Coelho, J., Pereira, B., Tarling, G., Pardal, M., Bustamante, P., Stowasser, G., Brierley, A., Pereira, M., 2019. Spatial variability in total and organic mercury levels in Antarctic krill Euphausia superba across the Scotia Sea. Environ Pollut 247, 332–339.
[80] Korejwo, E., Panasiuk, A., Wawrzynek-Borejko, J., Jedruch, A., Beldowski, J., Paturej, A., Beldowska, M., 2023. Mercury Conc Antarct zooplankton a Focus krill Species, Euphausia superba, Sci Tot Environ 905 (167239).
[81] Chouvelon, T., Warnau, M., Churlaud, C., Bustamante, P., 2009. Hg concentrations and related risk assessment in coral reef crustaceans, molluscs and fish from New Caledonia. Environ Pollut 157, 331–340.
[82] Hintelmann, H., Nguyen, H.T., 2005. Extraction of methylmercury from tissue and plant samples by acid leaching. Anal Bioanal Chem 381, 360–365.
[83] Janssen, S.E., Lepak, R.F., Tate, M.T., Ogorek, J.M., DeWild, J.F., Babiarz, C.L., Hurley, J.P., Krabbenhoft, D.P., 2019. Rapid pre-concentration of mercury in solids and water for isotopic analysis. Anal Chim Acta 1054, 95–103.
[84] Blum, J.D., Bergquist, B.A., 2007. Reporting of variations in the natural isotopic composition of mercury. Anal Bioanal Chem 388, 353–359.
[85] Blum, J.D., Johnson, M.W., 2017. Recent Developments in Mercury Stable Isotope Analysis. In: Teng, F.Z., Watkins, J., Dauphas, N. (Eds.), Non-Traditional Stable Isotopes, Mineralogical Society of America. Washington, DC, pp. 733–757.
[86] Rosera, T.J., Janssen, S.E., Tate, M.T., Lepak, R.F., Ogorek, J.M., DeWild, J.F., Babiarz, C.L., Krabbenhoft, D.P., Hurley, J.P., 2020. Isolation of methylmercury using distillation and anion-exchange chromatography for isotopic analyses in natural matrices. In: Anal. Bioanal. Chem, 412, pp. 681–690.
[87] Glatzel, P., Harris, A., Marion, P., Sikora, M., Weng, T.C., Guilloud, C., Lafuerza, S., Rovezzi, M., Detlefs, B., Ducotté, L., 2021. The five-analyzer point-to-point scanning crystal spectrometer at ESRF ID26. J Synchrotron Rad 28, 362–371.
[88] Glatzel, P., Weng, T.C., Kvashnina, K., Swarbrick, J., Sikora, M., Gallo, E., Smolentsev, N., Mori, R.A., 2013. Reflections on hard X-ray photon-in/photon-out spectroscopy for electronic structure studies. J Electron Spectrosc 188, 17–25.
[89] Manceau, A., Enescu, M., Simionovici, A., Lanson, M., Gonzalez-Rey, M., Rovezzi, M., Tucoulou, R., Glatzel, P., Nagy, K.L., Bourdineaud, J.-P., 2016. Chemical forms of mercury in human hair reveal sources of exposure. Environ Sci Technol 50, 10721–10729.
[90] Nehzati, S., Dolgova, N.V., Young, C.G., James, A., Cotelesage, J.J.H., Sokaras, D., Kroll, T., Qureshi, M., Pickering, I.J., George, G.N., 2022. Mercury Lα1 high energy resolution fluorescence detected X-ray absorption spectroscopy: a versatile speciation probe for mercury. Inorg Chem 61, 5201–5214.
[91] Rovezzi, M., Lapras, C., Manceau, A., Glatzel, P., Verbeni, R., 2017. High energy-resolution x-ray spectroscopy at ultra-high dilution with spherically bent crystal analyzers of 0.5 m radius. Rev Sci Instr 88 (013108).
[92] Sole, V.A., Papillon, E., Cotte, M., Walter, P., Susini, J., 2007. A multiplatform code for the analysis of energy-dispersive X-ray fluorescence spectra. Spectrochim Acta, B 62, 63–68.
[93] Hopke, P.K., 1989. Target transformation factor analysis. Chemom Intell Lab Syst 6, 7–19.
[94] Manceau, A., Marcus, M., Lenoir, T., 2014. Estimating the number of pure chemical components in a mixture by X-ray absorption spectroscopy. J Synchrotron Radiat 21, 1140–1147.
[95] Pickering, I.J., Cheng, Q., Rengifo, E.M., Nehzati, S., Dolgova, N.V., Kroll, T., Sokaras, D., George, G.N., Arner, E.S.J., 2020. Direct observation of methylmercury and auranofin binding to selenocysteine in thioredoxin reductase. Inorg Chem 59, 2711–2718.
[96] de Maria, M., Lamarche, J., Ronga, L., Messori, L., Szpunar, J., Lobinski, R., 2023. Selenol (-SeH) as a target for mercury and gold in biological systems: contributions of mass spectrometry and atomic spectroscopy. Coord Chem Rev 474 (214836).
[97] El Hanafi, K., Fernadez-Bautista, T., Ouerdane, L., Corns, W.T., Bueno, M., Fontagné-Dicharry, S., Amouroux, D., Pedrero, Z., 2024. Exploring mercury detoxification in fish: the role of selenium from tuna byproduct diets for sustainable aquaculture. J Hazard Mater 480 (135779).
[98] Madabeni, A., Bortoli, M., Nogara, P.A., Ribaudo, G., Tiezza, M.Dalla, Flohé, L., Rocha, J.B.T., Orian, L., 2024. 50 years of organoselenium chemistry, biochemistry and reactivity: mechanistic understanding, successful and controversial stories. Chem Eur J (in press.).
[99] Malinowski, E.R., 1978. Theory of error for target factor analysis with applications to mass spectrometry and nuclear magnetic resonance spectrometry. Anal Chim Acta 103, 359–354.
[100] Smichowski, P., Vodopivez, C., Muñoz-Olivas, R., Gutierrez, A.M., 2006. Monitoring trace elements in selected organs of Antarctic penguin (*Pygoscelis adeliae*) by plasma-based techniques. Microchem J 82, 1–7.
[101] Carravieri, A., Bustamante, P., Churlaud, C., Cherel, Y., 2013. Penguins as bioindicators of mercury contamination in the Southern Ocean: birds from the Kerguelen Islands as a case study. Sci Tot Environ 454, 141–148.
[102] Brasso, R., Polito, M., Lynch, H., Naveen, R., Emslie, S., 2012. Penguin eggshell membranes reflect homogeneity of mercury in the marine food web surrounding the Antarctic Peninsula. Sci Tot Environ 439, 165–171.
[103] Brasso, R., Polito, M., Emslie, S., 2014. Multi-tissue analyses reveal limited inter-annual and seasonal variation in mercury exposure in an Antarctic penguin community. Ecotoxicology 23, 1494–1504.
[104] Carravieri, A., Cherel, Y., Blevin, P., Brault-Favrou, M., Chastel, O., Bustamante, P., 2014. Mercury exposure in a large subantarctic avian community. Environ Poll 190, 51–57.
[105] Carravieri, A., Cherel, Y., Jaeger, A., Churlaud, C., Bustamante, P., 2016. Penguins as bioindicators of mercury contamination in the southern Indian Ocean: geographical and temporal trends. Environ Pollut 213, 195–205.
[106] Polito, M., Brasso, R., Trivelpiece, W., Karnovsky, N., Patterson, W., Emslie, S., 2016. Differing foraging strategies influence mercury (Hg) exposure in an Antarctic penguin community. Environ Pollut 218, 196–206.
[107] Calizza, E., Signa, G., Rossi, L., Vizzini, S., Careddu, G., Tramati, C., Sporta Caputi, S., Mazzola, A., Costantini, M., 2021. Trace elements and stable isotopes in penguin chicks and eggs: a baseline for monitoring the Ross Sea MPA and trophic transfer studies. Mar Pollut Bull 170 (112667).
[108] Wagemann, R., Trebacz, E., Boila, G., Lockhart, W.L., 1998. Methylmercury and total mercury in tissues of arctic marine mammals. Sci Tot Environ 218, 19–31.
[109] Evers, D.C., Savoy, L.J., DeSorbo, C.R., Yates, D.E., Hanson, W., Taylor, K., Siegel, L.S., Cooley, J.H., Bank, M.S., Major, A., Munney, K., Mower, B.F., Vogel, H.S., Schoch, N., Pokras, M., Goodale, M.W., Fair, J., 2008. Adverse effects from environmental mercury loads on breeding common loons. Ecotoxicol 17, 69–81.
[110] Lavoie, R.A., Jardine, T.D., Chumchal, M.M., Kidd, K.A., Campbell, L.M., 2013. Biomagnification of mercury in aquatic food webs: a worldwide meta-analysis. Environ Sci Technol 47, 13385–13394.
[111] Seco, J., Aparício, S., Brierley, A.S., Bustamante, P., Ceia, F.R., Coelho, J.P., Philips, R.A., Saunders, R.A., Fielding, S., Gregory, S., Matias, R., Pardal, M.A., Pereira, E., Stowasser, G., Tarling, G.A., Xavier, J.C., 2021. Mercury biomagnification in a Southern Ocean food web. Environ Pollut 275 (116620).
[112] de Ferro, A.M., Mota, A.M., Canário, J., 2014. Pathways and speciation of mercury in the environmental compartments of Deception Island, Antarctica. Chemosphere 95, 227–233.

[113] Pilcher, N., Gaw, S., Eisert, R., Horton, T., Gormley, A., Cole, T., Lyver, P., 2020. Latitudinal, sex and inter-specific differences in mercury and other trace metal concentrations in Adelie and Emperor penguins in the Ross Sea, Antarctica. Mar Pollut Bull 154 (111047).
[114] Cusset, F., Bustamante, P., Carravieri, A., Bertin, C., Brasso, R., Corsi, I., Dunn, M., Emmerson, L., Guillou, G., Hart, T., Juáres, M., Kato, A., Machado-Gaye, A.L., Michelot, C., Olmastroni, S., Polito, M., Raclot, T., Santos, M., Schmidt, A., Southwell, C., Soutullo, A., Takahashi, A., Thiebot, J., Trathan, P., Vivion, P., Waluda, C., Fort, J., Cherel, Y., 2023. Circumpolar assessment of mercury contamination: the Adélie penguin as a bioindicator of Antarctic marine ecosystems. Ecotoxicol 32, 1024–1049.
[115] Magat, W., Sell, J.L., 1979. Distribution of mercury and selenium in egg components and egg-white proteins. Proc Soc Exp Biol Med 161, 458–463.
[116] Kennamer, R.A., Stout, J.R., Jackson, B.P., Colwell, S.V., Brisbin, I.L., Burger, J., 2005. Mercury patterns in wood duck eggs from a contaminated reservoir in South Carolina, USA. Environ Toxicol Chem 24, 1793–1800.
[117] Bond, A.L., Diamond, A.W., 2009. Total and methyl mercury concentrations in seabird feathers and eggs. Arch Environ Contam Toxicol 56, 286–291.
[118] Ackerman, J.T., Herzog, M.P., Schwarzbach, S.E., 2013. Methylmercury is the predominant form of mercury in bird eggs: a synthesis. Environ Sci Technol 47, 2052–2060.
[119] Charrier, J., Fort, J., Tessier, E., Asensio, O., Guillou, G., Grémillet, D., Marsaudon, V., Gentès, S., Amouroux, D., 2024. Mercury compound distribution and stable isotope composition in the different compartments of seabird eggs: The case of three species breeding in East Greenland. Chemosphere 363 (142857).
[120] Ackerman, J.T., Herzog, M.P., Evers, D.C., Cristol, D.A., Kenow, K.P., Heinz, G.H., Lavoie, R.A., Brasso, R.L., Mallory, M.L., Provencher, J.F., Braune, B.M., Matz, A., Schmutz, J.A., Eagles-Smith, C.A., Savoy, L.J., Meyer, M.W., Hartman, C.A., 2020. Synthesis of maternal transfer of mercury in birds: implications for altered toxicity risk. Environ Sci Technol 54, 2878–2891.
[121] Hill, K.E., Zhou, J., Austin, L.M., Motley, A., Ham, A.J.L., Olson, G.E., Atkins, J.F., Gesteland, R., Burk, R.F., 2007. The selenium-rich C-terminal domain of mouse selenoprotein P is necessary for the supply of selenium to brain and testis but not for the maintenance of whole body selenium. J Biol Chem 282, 10972–10980.
[122] Kooyman, G.L., Kooyman, T.G., 1995. Diving behavior of emperor penguins nurturing chicks at Coulman Island, Antarctica. Condor 97, 536–549.
[123] Perrot, V., Masbou, J., Pastukhov, M.V., Epov, V.N., Point, D., Berail, S., Becker, P.R., Sonke, J.E., Amouroux, D., 2016. Natural Hg isotopic composition of different Hg compounds in mammal tissues as a proxy for in vivo breakdown of toxic methylmercury. Metallomics 8, 170–178.
[124] El Hanafi, K., Pedrero, Z., Ouerdane, L., Moreno, C.M., Queipo-Abad, S., Bueno, M., Pannier, F., Corns, W.T., Cherel, Y., Bustamante, P., Amouroux, D., 2022. First time identification of selenoneine in seabirds and its potential role in mercury detoxification. Environ Sci Technol 56, 3288–3298.
[125] Bosl, M.R., Takaku, K., Oshima, M., Nishimura, S., Taketo, M.M., 1997. Early embryonic lethality caused by targeted disruption of the mouse selenocysteine tRNA gene (Trsp). Proc Natl Acad Sci USA 94, 5531–5534.
[126] Burk, R.F., Olson, G.E., Hill, K.E., Winfrey, V.P., Motley, A.K., Kurokawa, S., 2013. Maternal-fetal transfer of selenium in the mouse. FASEB J 27, 3249–3256.
[127] Tujebajeva, R., Ransom, D., Harney, J., Berry, M., 2000. Expression and characterization of nonmammalian selenoprotein P in the zebrafish, *Danio rerio*. Genes Cells 5, 897–903.
[128] Barkay, T., Gu, B., 2021. Demethylation—the other side of the mercury methylation coin: a critical review. ACS Environ Au 2, 77–97.
[129] Panhou, H.S.K., Imura, N., 1981. Biotransformation of Mercurials by Intestinal Microorganisms Isolated from Yellowfin Tuna. Bull Environ Contam Toxicol 26, 359–363.
[130] Kritee, K., Barkay, T., Blum, J.D., 2009. Mass dependent mercury stable isotope fractionation during mer mediated microbial degradation of monomethylmercury. Geochim Cosm Acta 73, 1285–1296.
[131] Lafrance-Vanasse, J., Lefebvre, M., Di Lello, P., Sygusch, J., Omichinski, J.G., 2009. Crystal structures of the organomercurial lyase MerB in its free and mercury-bound forms: insights into the mechanism of methylmercury degradation. J Biol Chem 284, 938–944.
[132] Parks, J.M., Guo, H., Momany, C., Liang, L.Y., Miller, S.M., Summers, A.O., Smith, J.C., 2009. Mechanism of Hg-C protonolysis in the organomercurial Lyase MerB. J Am Chem Soc 131, 13278–13285.
[133] Goutte, A., Bustamante, P., Barbraud, C., Delord, K., Weimerskirch, H., Chestel, O., 2014. Demographic responses to mercury exposure in two closely related Antarctic top predators. Ecology 95, 1075–1086.
[134] Carravieri, A., Cherel, Y., Brault-Favrou, M., Churlaud, C., Peluhet, L., Labadie, P., Budzinski, H., Chastel, O., Bustamante, P., 2017. From Antarctica to the subtropics: Contrasted geographical concentrations of selenium, mercury, and persistent organic pollutants in skua chicks (Catharacta spp.). Environ. Pollut. 228, 464–473.